Field Crops Research 284 (2022) 108579

Contents lists available at ScienceDirect

Field Crops Research

journal homepage: www.elsevier.com/locate/fcr

Crop yield estimation and irrigation scheduling optimization using a root-weighted soil water availability based water production function

Xun Wu [a,d,e], Jianchu Shi [a,d,e], Ting Zhang [a,d,e], Qiang Zuo [a,d,e,*], Lichun Wang [b], Xuzhang Xue [b], Alon Ben-Gal [c]

[a] College of Land Science and Technology, China Agricultural University, Beijing 100193, China
[b] National Research Center of Intelligent Equipment for Agriculture, Beijing 100097, China
[c] Soil, Water and Environmental Sciences, Agricultural Research Organization – Volcani Institute, Gilat Research Center, mobile post Negev 85280, Israel
[d] Key Laboratory of Plant-Soil Interactions, Ministry of Education, Beijing 100193, China
[e] Key Laboratory of Arable Land Conservation (North China), Ministry of Agriculture, Beijing 100193, China

ARTICLE INFO

Keywords:
Crop-water production function
Root-weighted plant water deficit index
Cumulative function of water sensitivity index
Regulated deficit irrigation
Winter wheat

ABSTRACT

The crop-water production function (CWPF) is widely used to quantitatively describe relationships between crop water deficit and yield, and evaluate the effects of different irrigation strategies in agro-hydrological models. In order to reasonably and reliably estimate crop yield and optimize irrigation scheduling, a novel CWPF was proposed by combining the plant water deficit index (PWDI), estimated based on root-weighted soil water availability, with a daily water sensitivity index derived from a sigmoidal cumulative function. Parameterized using data from a two-year winter wheat field lysimetric experiment conducted in the North China Plain and from a previously published two-year spring maize field drip irrigation experiment in Inner Mongolia, China, the CWPFs provided reasonable estimation of different crop yields with different water stress response characteristics under different field environments. Through coupling the genetic algorithm with the integrated simulations of soil water dynamics, PWDI and CWPF in the soil-wheat system, an optimization procedure was developed to determine PWDI threshold combinations to timely trigger irrigation according to pre-designed crop water deficit status. Crop yield and water use efficiency (WUE) of winter wheat were estimated and compared under different optimized constant and variable PWDI threshold combinations. In addition, the effects of climate change on the optimized variable PWDI threshold combinations were investigated using 38 years of historic meteorological data. The results showed that regulated deficit irrigation (RDI) with a variable threshold combination, in which the sensitivity characteristics to water deficit were considered for the crop at different growth stages, was superior to a constant threshold in enhancing crop yield and WUE. Irrespective of the number of irrigation events (1, 2, 3 or 4) during the growing season, the coefficients of variation (CV) of optimized PWDI thresholds for different combinations of irrigation sequence and events were not very large under the same kind of hydrological year (wet, normal or dry), with CV < 0.39 and a median of 0.21. When the mean (MN) of the optimized PWDI threshold combinations for different irrigation sequence and events was used to schedule RDI of winter wheat in terms of various hydrological years, up to 91% of the estimated relative yield was found to be higher than 90% of the corresponding maximum values. Therefore, the MN can be valuable in formulating rational irrigation management strategies of winter wheat to achieve relatively high yields with limited water under changing climatic conditions.

Abbreviations: CWPF, crop-water production function; PWDI, plant water deficit index; WUE, water use efficiency; RWU, root water uptake; RLD, root length density; NRLD, normalized root length density; DAS, days after sowing; SWC, soil water content; GA, genetic algorithm; MN, mean; CV, coefficient of variation; NSE, Nash-Sutcliffe efficiency coefficient; RMSE, root mean squared error.

* Corresponding author at: College of Land Science and Technology, China Agricultural University, Beijing 100193, China.
E-mail addresses: wuxun232425@163.com (X. Wu), shijianchu@cau.edu.cn (J. Shi), tzztsn@163.com (T. Zhang), qiangzuo@cau.edu.cn (Q. Zuo), wanglc@nercita.org.cn (L. Wang), xuexz@nercita.org.cn (X. Xue), bengal@volcani.agri.gov.il (A. Ben-Gal).

https://doi.org/10.1016/j.fcr.2022.108579
Received 23 November 2021; Received in revised form 10 April 2022; Accepted 16 May 2022
Available online 23 May 2022

1. Introduction

Due to growing competition from cities, industry, and the environment for limited fresh water resources, scarcity of water for agriculture is becoming an increasingly serious problem in arid and semiarid regions (Elliott et al., 2014). Efficient water use in crop production, which is greatly dependent on proper irrigation scheduling to influence water use by the crop and its final yield, is vital for the development of sustainable agriculture. To pursue relatively high crop yield and water use efficiency (WUE) with a limited water supply, irrigation scheduling is often determined based on time-consuming and costly large-scale field irrigation experiments. However, results of such experiments are often only suitable for the specific soil and climatic conditions in which they were conducted (Arora et al., 1987). Numerical simulations offer an alternative more efficient and economic method to schedule irrigation by quantifying the relationship between crop yield/WUE and irrigation water. Such use of numerical simulations to optimize irrigation scheduling has gained popularity over the last decades (Shi et al., 2020, 2021; Dabach et al., 2013).

Models, including those driven by radiation, carbon, and/or water, have been developed to simulate crop growth and yield formation under various irrigation regimes (Diepen et al., 1989; Jones et al., 2003; Steduto et al., 2009). These models often require comprehensive and complicated, and quite difficult to determine, input parameters associated with various physiological processes (e.g. photosynthesis, transpiration, and respiration). In comparison, through directly and empirically relating crop yield to water availability, a crop-water production function (CWPF) greatly simplifies the estimation of crop yield by using a readily obtained variable such as irrigation amount (Stewart and Hagan, 1973), soil water storage (Morgan et al., 1980; Huang, 2004), evapotranspiration (Jensen, 1968; Igbadun et al., 2007) or transpiration (Hanks and Hill, 1980; Woli et al., 2014). CWPFs have been extensively employed by different agro-hydrological models to evaluate pre-designed irrigation strategies (Oweis and Hachum, 2009; Smilovic et al., 2016). Among the variables used to represent water availability, transpiration (T_a) should be one of the most appropriate parameters for assessing crop yield since T_a is closely related to photosynthetic assimilation (essentially a physiological water-consuming process) and yield formation (Ben-Gal et al., 2003). Generally, T_a is estimated by taking into account information such as meteorological data, leaf area index and average root-zone soil water content (SWC) or potential, as demonstrated by the classic Penman-Monteith formula (Allen et al., 1998; Lai and Katul, 2000). In this method, only the effect of soil water amount on crop water use is considered, while the effect of relative distribution pattern of soil water to roots is ignored, likely resulting in inaccurate estimation of T_a (Lai and Katul, 2000; Shi et al., 2015). In order to overcome this shortcoming, T_a can be estimated using a root water uptake (RWU) model based on root distribution (Jarvis, 1989; Šimůnek and Hopmans, 2009). Thereupon, different forms of CWPFs are constructed according to the relationship between relative yield and relative T_a during the whole growth season or by stages. Compared to season-based CWPF, stage-based functions better capture the differences in water sensitivity of crops at different growing periods and more reasonably describe the relationship between crop yield and T_a (Ben-Gal et al., 2003; Foster and Brozovi, 2018). Nevertheless, the application of stage-based CWPFs in agricultural production is still subject to some critical limitations as follows.

First, root information, usually characterized by root length density (RLD) distribution, while indispensable for a RWU model to estimate crop transpiration and to evaluate crop water deficit, is difficult and time-consuming to acquire reliably, especially in the field. It is fortunate to find that the distribution of normalized RLD (NRLD) vs. normalized root depth for a number of specific crops (e.g. wheat, cotton, maize, and rice) could be statistically described using a general function, independent of soil properties, crop species, growing stages, climate, and other environmental conditions (Wu et al., 1999; Zuo et al., 2013; Ning et al., 2015). By introducing NRLD as a weighting factor for available soil water in the root zone, a root-weighted plant water deficit index (PWDI) was put forward to characterize the extent of crop water deficit (Shi et al., 2015). The index was reliable in estimating T_a conveniently and accurately, and thus should be helpful for constructing a CWPF to predict crop yield under various water deficit scenarios.

Moreover, the sensitivity index (λ) for each growth stage is an important parameter in stage-based CWPFs. Its optimization often depends on laborious field experiments with various irrigation treatments. The accuracy of λ is susceptible to the artificial division of growth stages, which is usually subjective or even arbitrary. More specifically, too few growth stage divisions (i.e. long intervals) may be detrimental to capture the water sensitive response dynamics of crops, which likely results in the lack of sensitivity information in some key growth periods, and makes the triggering or scheduling of irrigation untimely or irrational. However, too many growth stage divisions (short intervals) can easily lead to instability, non-unique or even exceeding the reasonable range (such as negative values) of the optimized λ. A few research results showed that a cumulative function would be useful to determine λ at different timescales (Shang and Mao, 2006; Han et al., 2010). A typically low-high-low bell-shaped distribution of λ changing with time has been observed over the whole growth period for a variety of crops such as wheat, maize, cotton, soybean and rice. Its cumulative process over time was roughly in line with an S-shaped curve and able to be well described using a sigmoidal or logistic cumulative function (Kipkorir and Raes, 2002; Georgiou and Papamichail, 2008). The effect of water deficit on yield formation is a continuous process with crop growth. Therefore, the employment of a sigmoidal cumulative function should be physically sound and enable robust estimation of λ at a small timescale (e.g. daily) on the basis of solving problems such as missing sensitivity information and instability of optimization caused by artificial growth stage divisions. In summary, it would be wise to establish a novel CWPF combining a PWDI (used to indicate the degree of crop water deficit) estimated based on root-weighted soil water availability and a sigmoidal cumulative function (used to evaluate the daily water sensitivity index λ). However, the accuracy and reliability of this method in estimating crop yield awaits further research.

CWPFs have been widely used for optimizing the irrigation quota in each pre-designed growth stage, but rarely for determining the specific irrigation frequency, which should be dependent on the degree of crop water deficit or PWDI. Undoubtedly, choosing a reasonable PWDI threshold is critical for initiating each irrigation event. Both crop yield and WUE are found to change with changing PWDI thresholds. The relationships, usually obtained through irrigation experiments (Irmak et al., 2000; Emekli et al., 2007; Candogan et al., 2013; Shi et al., 2020) or numerical simulations (Shi et al., 2021), can be used to optimize the PWDI threshold, whether chosen as constant throughout the growth season or variable according to artificially pre-designed growth stages. However, due to the limited experimental conditions or simulation scenarios, the thresholds would represent a local optimum under those pre-designed conditions or scenarios, but not a global optimum for all possible situations. In addition, optimized PWDI thresholds, whether constant or variable, often originate from a specific seasonal climatic condition, without any consideration of the impact of climate change. Influenced by intra and inter seasonal climatic variability, the root-zone soil water availability for PWDI estimation is likely to change continuously and significantly, thus resulting in constantly changing PWDI thresholds optimized during various seasons, which are hard to be applied to trigger irrigation in practice. Therefore, it is necessary to investigate and evaluate the effect of changing climatic conditions on PWDI threshold optimization.

A truly global optimum PWDI threshold acquired from the proposed CWPF necessitates the incorporation of optimization algorithms (Singh and Panda, 2013; Singh, 2014). The genetic algorithm (GA) is a global search optimization procedure based on the mechanism of natural selection and genetics combining artificial survival of the fittest with

genetic operators (Holland, 1975). With the significant advantages of high efficiency and strong robustness in parallel computation, the GA has become a powerful tool for highly complex optimization problems (Wang et al., 2010; Sotomayor et al., 2018) and should be more suitable for optimizing PWDI thresholds based on CWPF than other traditional optimization algorithms such as linear programming, dynamic programming or Simplex method (Wen et al., 2017; Li et al., 2018a).

In summary, accurate evaluation of crop water deficit and water sensitivity is critical for reasonably constructing a CWPF and thereby for optimization of irrigation scheduling through a global search optimization algorithm like GA. It would be helpful to delineate the extent of crop water deficit using a PWDI based on available soil water weighted by the NRLD distribution and to derive water sensitivity dynamics from the cumulative function of a water sensitivity index. Therefore, the main objectives of this study were to (1) construct a novel CWPF by combining root-weighted soil water availability based PWDI with a cumulative function of sensitivity index, and to evaluate its accuracy and reliability in predicting crop yield using two multi-year field experiments on different crops (winter wheat and spring maize) under different climatic zones (Beijing and Inner Mongolia), soil types (loam and sandy), and irrigation methods (surface and drip irrigation); and (2) develop an optimization procedure of PWDI threshold determination and use by coupling GA into the integrated model including the simulations of soil water dynamics, PWDI and CWPF, and apply it to investigate and analyze the differences of crop yield and WUE resulting from irrigation scheduling controlled by either constant or variable PWDI irrigation thresholds or from the effects of changes in meteorological conditions due to climate change.

2. Materials and methods

2.1. Field lysimetric experiment

2.1.1. Experimental site and design

Data from a two-year field lysimetric experiment conducted in the North China Plain from September 2014 and 2015 to June the next year were used to parameterize and evaluate a CWPF based on root-weighted soil water availability. The field work was carried out at the National Experimental Station for Precision Agriculture in Changping District, Beijing (40°10′31′ N, 116°26′10′′ E, altitude 50.1 m), a warm temperate continental monsoon climate zone with 185 annual mean frost-free days, sunshine duration of 2600 h, and precipitation of 543 mm, of which 70% falls in the period between June and September. Supplemental irrigation is necessary in the region for agricultural production of winter wheat sown at the end of September and harvested in early June of the next year. Additional details regarding the experimental site were presented in Wu et al. (2017).

On 29 September 2014 and 2015, winter wheat (*Triticum aestivum* L. *Nongda* 212) was sown in 14 weighing lysimeters (230 cm high × 75 cm wide × 100 cm long, 0.05 mm in precision) at a density of 6.7×10^6 plants ha^{-1}. Space around the lysimeters was also planted at the same density to avoid margin effects. Layout of lysimeters in the field was detailed in Wu et al. (2020). Before sowing, all lysimeters were uniformly watered in order to maintain optimal soil water conditions for the growth of winter wheat during seedling stage. The steel box of each lysimeter was filled in by excavating original soil monoliths taken from a nearby field, with three undisturbed distinct loam soil layers (Table 1). Soil physical properties were measured using the following standard methods: the gravitational liquid sedimentation technique for soil particle composition (Gee and Or, 2002); constant head method for saturated hydraulic conductivity (Klute and Dirksen, 1986); and pressure membrane plate for soil water retention characteristics (Soil Moisture Equipment Co., USA), fitted through the closed-form equation of van Genuchten (1980) and used to obtain the field capacity as the SWC corresponding to the soil matric potential of − 300 cm (Romano and Santini, 2002). Totally six (T1, T2, T3, T4, T5 and T6, 2014–2015) and seven (T7, T8, T9, T10, T11, T12 and T13, 2015–2016) irrigation treatments were respectively designed for the two growth seasons of winter wheat. The dates and amount of irrigation for each treatment are detailed in Table 2. For treatments T1 and T7, irrigation was applied every 1–3 d from 203 and 191 days after sowing (DAS), respectively, to maintain sufficient water supply for the growth of winter wheat. Treatments T6 and T13 were fully covered by plastic film and did not receive any irrigation during the season. Rainfall was completely

Table 2
Irrigation treatments and schedules during the growing season of winter wheat from 2014 to 2016. DAS = days after sowing.

Growing season	Treatments	Date (DAS)	Irrigation depth (cm)
Sep. 2014-Jun. 2015	T1	47	5.1
		203–240	Irrigated every 1–3 d, 37.6 cm in total
	T2	47	5.1
		215	4.5
		229	5.1
		238	6.3
	T3	47	7.2
		197	7.2
		217	7.2
	T4	47	7.2
		197	7.2
	T5	47	7.2
	T6	Film mulched without any irrigation	
Sep. 2015-Jun. 2016	T7	47	3.0
		188	5.1
		191–240	Irrigated every 1–3 d, 60.7 cm in total
	T8	47	3.0
		188	5.1
		196	7.4
		207	6.7
		222	8.1
		234	8.1
	T9	47	3.0
		188	5.1
		213	9.6
		233	9.7
	T10	47	7.2
		201	7.2
		218	7.2
		234	7.2
	T11	47	7.2
		201	7.2
		218	7.2
	T12	47	7.2
	T13	Film mulched without any irrigation	

Table 1
Soil properties: texture (content of sand, silt, and clay), bulk density (ρ_b), saturated water content (θ_s), field water capacity (θ_f), residual water content (θ_r), saturated hydraulic conductivity (K_s), and the fitting parameters (α and n) in van Genuchten's (1980) soil water retention curve.

Depth	Sand	Silt	Clay	ρ_b	θ_s	θ_r	θ_f	K_s	α	n
(cm)	(%)	(%)	(%)	(g cm^{-3})	(cm^3 cm^{-3})	(cm^3 cm^{-3})	(cm^3 cm^{-3})	(cm d^{-1})	(cm^{-1})	
0–30	49.44	45.04	5.52	1.43	0.495	0.029	0.316	5.13	0.014	1.315
30–80	34.82	44.20	20.98	1.40	0.541	0.068	0.394	1.86	0.013	1.245
80–230	31.92	49.90	18.18	1.56	0.548	0.060	0.410	0.12	0.020	1.177

prevented by a movable rain-shelter from greening until harvest.

2.1.2. Measurements

Data collected during the field lysimetric experiment included meteorological data, SWC and crop information, which were obtained through the methods or procedures respectively described as follows.

(1) Meteorological data: Meteorological data at study site (including air temperature, relative humidity, solar radiation, and wind speed) were monitored and recorded by an automatic agro-meteorological station (WeatherHawk 500, Campbell Scientific, USA).

(2) SWC: At the wheat turning green stage (168 DAS), the SWC was measured by a calibrated capacitance probe (Diviner 2000, Sentek, Australia) at 10 cm intervals from soil surface to 160 cm depth. This was used as the initial condition to verify the soil water transport model. From heading (2015) or jointing (2016) to maturity (198–244 DAS; 188–244 DAS), the SWC in each lysimeter was measured daily to estimate PWDI dynamics.

(3) Crop information:

- Leaf area: Five winter wheat plants from each lysimeter were randomly pre-selected to measure the length and width of green leaves at a 5–7 d interval, and then leaf area was calculated as a product of the measured length, width and a measured conversion coefficient of 0.77 (Wu et al., 2017).
- Transpiration: Daily actual transpiration rate under each treatment was determined by deducting actual soil evaporation rate (under the treatments other than film mulched T6 and T13), estimated according to weather data, leaf area index and surface SWC using the modified Penman equation (Ritchie, 1972; Wu et al., 1999), from actual evapotranspiration rate obtained through weighing. The actual soil evaporation rate was assumed to be negligible for the film mulched treatments of T6 and T13.
- Grain yield: All the winter wheat plants in each lysimeter were removed to measure grain yield at harvest.

2.2. Theoretical background

2.2.1. Crop-water production function (CWPF)

A multiplicative approach proposed by Rao et al. (1988) was employed to relate relative yield (Y_a/Y_p) to relative transpiration rates (T_a/T_p) of different growth stages, viz.

$$Y_a/Y_p = \prod_{i=1}^{n}\left(1-\lambda_i\left(1-T_a/T_p\right)_i\right) \quad (1)$$

where Y_a and Y_p are actual and potential yields, respectively (kg ha^{-1}); T_a and T_p are averages of actual and potential transpiration rates during the ith ($i = 1, 2, 3, \ldots, n$) growth stage (mm d^{-1}), respectively, and n is the number of growth stage divisions; 1 - T_a/T_p is the plant water deficit index (PWDI) representing the extent of crop water deficit (Woli et al., 2012; Shi et al., 2015); λ_i is the sensitivity index of the ith stage.

As aforementioned, the application of Eq. (1) suffers from lack of consideration regarding the effect of root distribution on T_a estimation, and subjective or even arbitrary division of specific growth stages. A recently proposed root-weighted PWDI was useful to improve the estimation accuracy of the extent of crop water deficit by taking both soil water amount and relative distribution of soil water to roots into account (Shi et al., 2015). A sigmoidal cumulative function of sensitivity index provided an effective way to describe the response of yield formation to continuous water deficit dynamics and allowed the acquisition of sensitivity index at a daily timescale, which should be helpful for mitigating the adverse effects caused by the artificial division of growth stages (Shang and Mao, 2006; Han et al., 2010). Hence, root-weighted PWDI and cumulative function of sensitivity index were combined to revise Eq. (1) as:

$$Y_a/Y_p = \prod_{t=1}^{T}(1-\lambda_t \mathrm{PWDI}_t) \quad (2)$$

where t is the day after sowing (d); T is the number of days between sowing and maturity; PWDI_t is the root-weighted soil water availability based PWDI on the tth day (as described in Section 2.2.2); λ_t is the λ on the tth day, estimated with a sigmoidal cumulative function (as described in Section 2.2.3).

2.2.2. Root-weighted PWDI estimation

The PWDI based on root-weighted soil water availability was estimated as (Shi et al., 2015; Wu et al., 2017):

$$\mathrm{PWDI} = 1 - \int_0^1 \gamma(h) L_{nrd}(z_r)\mathrm{d}z_r \quad (3)$$

where h is the soil matric potential (cm); z_r (= z/L_r) is the normalized soil depth, i.e. the ratio of soil depth z (cm) to the maximum rooting depth L_r (cm), in which L_r is simulated by a root growth model relating the root penetration rate with the soil water content, sand content, bulk density and temperature as proposed by Asseng et al. (1997); $L_{nrd}(z_r)$ is the normalized root length density (NRLD); $\gamma(h)$ is the soil water stress response function quantifying the effect of soil water stress on RWU or transpiration, which can be expressed in linear (Feddes et al., 1978) or nonlinear (van Genuchten, 1987; Musters and Bouten, 1999; Homaee et al., 2002) forms. For the sake of simplicity, a piecewise linear function was chosen in this study (Feddes et al., 1978):

$$\gamma(h) = \begin{cases} 0 & h \geq h_H \\ 1 & h_L \leq h < h_H \\ \dfrac{h-h_W}{h_L-h_W} & h_W < h < h_L \\ 0 & h \leq h_W \end{cases} \quad (4)$$

where h_H, h_L and h_W are the thresholds of anaerobiosis point, optimal soil water condition and wilting point (cm), adopted according to the recommended values of − 50, − 400 and − 15,000 cm, respectively (Feddes et al., 1976). The parameters appearing in Section 2.2 and their values are summarized in Table 3 together with source references.

Since it was impossible to destructively sample roots during the growing season of winter wheat, a generalized function was utilized to estimate NRLD as (Zuo et al., 2013):

Table 3
Overview of the parameters contained in Section 2.2 and their sources.

Parameters	Unit	Meaning	Value	Source
h_H	cm	Anaerobiosis point	-50	Feddes et al. (1976)
h_L	cm	Threshold of optimal soil water condition	-400	Feddes et al. (1976)
h_W	cm	Wilting point	-15000	Feddes et al. (1976)
p	–	Shape parameter of NRLD distribution	3.85	Zuo et al. (2013)
H_m	℃	Potential heat units required for the maturation	1750	Measured
T_u	℃	Optimal temperatures for crop growth	30	Wang et al. (2013)
T_b	℃	Base temperatures for crop growth	0	Wang et al. (2013)
β	%	Percentage of wetting area	100	Measured
D_w	cm	Designed wetting depth	60	Wu et al. (2017)
k	–	Fitting parameter	23.38	Calibrated
b	–	Fitting parameter	3.53	Calibrated
m	–	Fitting parameter	1.04	Calibrated

$$L_{nrd}(z_r) = p(1 - z_r)^{p-1} \quad (5)$$

where p is a shape parameter denoting the NRLD at the soil surface, recommended as 3.85 for wheat by Zuo et al. (2013). The generalized function was established and tested using a large amount of measured NRLD data for wheat from published papers and their own experiments (1179 data points in total). The statistical analysis showed that the prediction uncertainty interval of the generalized function along the profile was within ± 0.16 under a confidence level of 95%, indicating that it should be feasible and reliable to be utilized in most cases (Wu et al., 2021).

2.2.3. Cumulative function of sensitivity index (λ)

The cumulative sensitivity index of λ can be (and has often been) expressed as a sigmoidal function of physical time such as days after emergence or sowing. However, due to the fact that the crop growth cycle (i.e. phenological phase) is highly dependent on changing environments (including meteorological conditions), the function is prone to be unstable and inapplicable especially when conditions fluctuate drastically. A normalized heat unit index (H_t, ranging between 0 and 1) calculated based on growing degree days (GDD) describes the crop growth cycle more stably than physical time (Ojeda-Bustamante et al., 2004). Thus, a more general sigmoidal curve was employed to describe the cumulative λ (named as C_t) as a function of H_t as follows (Han et al., 2010):

$$C_t = \frac{m}{1 + k(1/H_t - 1)^b} \quad (6)$$

where k, b and m are the fitting parameters. When $H_t \to 0$, $C_t \to 0$, denoting little sensitivity of crop yield to water deficit at sowing; when $0 < H_t < 1$, C_t increases with increasing H_t in an S-shape; when $H_t \to 1$, C_t changes little ($\to m$), indicating crop yield is insensitive to water deficit at maturity.

In Eq. (6), H_t was estimated as:

$$H_t = \frac{\sum_{i=1}^{t} GDD_i}{H_m} \quad (7)$$

in which,

$$GDD = \begin{cases} T_u - T_b & T_{ave} > T_u \\ T_{ave} - T_b & T_b \le T_{ave} \le T_u \\ 0 & T_{ave} < T_b \end{cases}$$

where T_{ave} is the average daily air temperature (°C); H_m is the potential heat units required for the maturation (°C), a cultivar- and environment-dependent parameter identified as 1750 °C for winter wheat according to the measurement in the lysimetric experiment; T_u and T_b are the optimal and base temperatures for crop growth, and set to 30 and 0 °C for winter wheat, respectively (Wang et al., 2013).

According to Eq. (6), daily λ (named as λ_t) was calculated as:

$$\lambda_t = C_t - C_{t-1} \quad (8)$$

2.2.4. Simulation of soil water dynamics

The Richards equation was employed to simulate one-dimensional vertical soil water flow in a soil-wheat system (van Genuchten, 1987):

$$C(h)\frac{\partial h}{\partial t} = \frac{\partial}{\partial z}\left[K(h)\left(\frac{\partial h}{\partial z} - 1\right)\right] - S(z,t) \quad (9)$$

$$h(z,\ 0) = h_0(z) \quad 0 \le z \le L \quad (10)$$

$$\left[-K(h)\left(\frac{\partial h}{\partial z} - 1\right)\right]_{z=0} = \varepsilon(t) \quad t > 0 \quad (11)$$

$$h(L,t) = \mathrm{h}_L(t) \quad t > 0 \quad (12)$$

where $C(h)$ is soil water capacity (cm^{-1}); $K(h)$ is unsaturated hydraulic conductivity (cm d^{-1}); $h_0(z)$ is the initial distribution of soil matric potential (cm); L ($\ge L_r$) is the simulation depth (cm); $h_L(t)$ is the soil matric potential at the lower boundary (cm); $\varepsilon(t)$ is the water flow rate from soil surface (cm d^{-1}), i.e. the infiltration rate of irrigation/precipitation water ($\varepsilon(t) > 0$) or evaporation rate ($\varepsilon(t) \le 0$); $S(z, t)$ is the actual RWU rate ($cm^3\ cm^{-3}\ d^{-1}$), estimated using a macroscopic RWU model as:

$$S(z,\ t) = \gamma(h)S_{\max}(z,\ t) = \frac{\gamma(h)T_p L_{nrd}(z_r)}{L_r} \quad (13)$$

where $S_{\max}(z, t)$ is the maximal RWU rate under optimal soil water condition ($cm^3\ cm^{-3}\ d^{-1}$). The potential transpiration rate (T_p) was computed as (Mailhol et al., 1997):

$$T_p = ET_p[1 - exp(-0.6LAI)] \quad (14)$$

where ET_p is the potential evapotranspiration rate (mm d^{-1}), estimated with the Penman-Monteith equation recommended by FAO-56 (Allen et al., 1998); LAI is the leaf area index ($cm^2\ cm^{-2}$).

2.2.5. Optimization of the PWDI threshold

Through coupling the optimization algorithm of GA with the integrated simulations including soil water dynamics (under various irrigation regimes), PWDI (estimated on the basis of simulated soil water dynamics) and CWPF (used to predict the final yields of different simulation scenarios), a procedure to optimize PWDI threshold was proposed as follows (Fig. 1):

(1) Define the objective function as maximizing the relative yield ($Y_r = Y_a/Y_p$):

$$\max\ Y_r = f(q, \mathbf{PWDI_v}) \quad (15)$$

$$0 \le \mathrm{PWDI}_v \le 1$$

where q is the irrigation times; $\mathbf{PWDI_v}$ is a q-dimension vector of PWDI threshold. The quota for each irrigation (I, cm) was determined according to the difference between the simulated SWC (θ, $cm^3\ cm^{-3}$) and

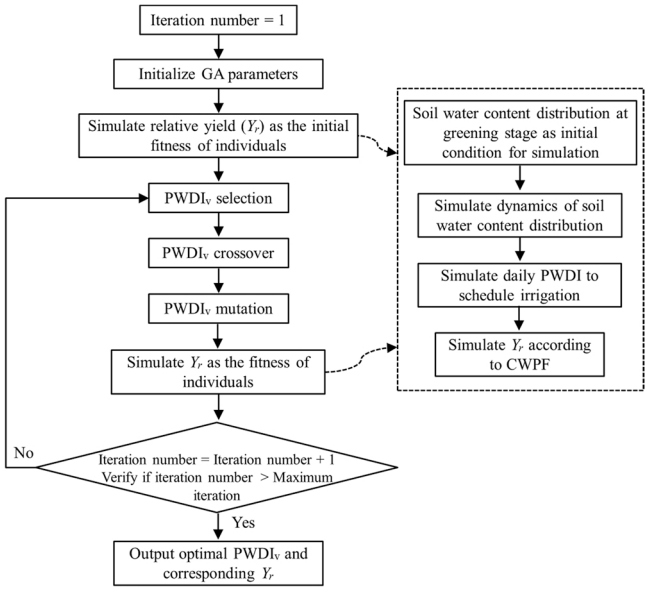

Fig. 1. Flow chart for optimizing plant water deficit index (PWDI) thresholds based on the genetic algorithm (GA). PWDI$_v$ is the combination or vector of variable PWDI threshold. CWPF is the crop-water production function.

field water capacity (θ_f, target water content, $cm^3\ cm^{-3}$) (Shi et al., 2015):

$$I = \beta \int_{z=0}^{D_w} [\theta_f - \theta(z,t)]dz \quad (16)$$

where β is the designed percentage of wetting area, fixed as 100% for surface irrigation in this study; D_w is the designed wetting depth (cm), set as 60 cm to prevent deep leakage (Wu et al., 2017).

(2) Initialize GA parameters. The population size, representing the number of individuals (i.e. $\mathbf{PWDI_v}$), was set to 50. The maximum iteration number of optimization was set to 80 to meet the computation requirement of stable solution. The crossover probability of 0.85 was chosen to ensure a relatively fast convergence to the global optimum. The mutation probability of 0.15 was used to avoid optimized results in local minima. The initial vector element values of first $\mathbf{PWDI_v}$ generation were automatically generated using the "rand" function provided by MATLAB software (R2014a, MathWorks Inc., MA, USA).

(3) Use the measured SWC at greening stage of winter wheat as the initial condition and simulate soil water dynamics (Eqs. (9) - (12)), estimate daily PWDI (Eq. (3)), and predict final Y_r (Eq. (2)). This Y_r was used as the initial fitness of individuals.

(4) Select the individual with the highest fitness from the previous generation individuals and move it to the next generation. The remaining individuals are then adjusted through crossover and mutation operations and moved to the next generation as well.

(5) Simulate the fitness (Y_r) of the newest generation individuals as described in Step (3), and repeat Step (4) to generate new individuals and transfer them into the next generation.

(6) Repeat Steps (4) and (5) until the real-time iteration number reached designed maximum value, and then output optimal $\mathbf{PWDI_v}$ and the corresponding Y_r (Fig. 1).

2.2.6. Simulation scenarios

The numerical simulation lasted from greening to maturity of winter wheat, with the measured SWC at greening stage in 2016 used as the initial condition of the scenario simulation. Two scenarios were set considering the effects of intra and inter seasonal climatic variability on the optimization of PWDI threshold, respectively. For the specific intra-season weather conditions observed at the field experimental station in 2016, two kinds of PWDI thresholds, constant and variable, were designed as follows:

- Constant threshold: During the simulation period, the PWDI threshold was kept as a constant, and increased from 0.01 to 0.99 with an interval of 0.01 to generate 99 cases. In each case, the SWC, PWDI, Y_r, and $IWUE_r$ (relative irrigation water use efficiency, i.e. the ratio of simulated IWUE to its maximum value) were simulated, respectively. The irrigation water use efficiency IWUE ($kg\ m^{-3}$) was calculated to evaluate the practical productivity of total irrigation water input as:

$$IWUE = 0.01 Y_a \Big/ \sum_{i=1}^{q} I_i \quad (17)$$

where I_i is the quota of the ith irrigation (cm).

- Variable threshold: Considering that there are usually no more than four irrigation events for winter wheat after the greening stage in the North China Plain, we designed four irrigation schemes with winter wheat irrigated 1, 2, 3 and 4 times, and then utilized the optimization procedure to determine the optimal PWDI threshold combination as well as the corresponding Y_r and $IWUE_r$.

The impact of inter seasonal meteorological variability was explored according to the local hydrological year (i.e., wet, normal, and dry year with precipitation frequency P = 0–25%, 25–75%, and 75–100%, respectively), which was based on 38 years (1981–2018) of historic daily meteorological data (e.g. maximum and minimum air temperature, relative air humidity, precipitation, wind speed, and solar radiation) from a nearby meteorological observation station of the experimental station. The numerical simulation also started from the measured SWC distribution at greening stage in 2016, and optimized variable PWDI threshold under four irrigation schemes with 1–4 irrigation events.

3. Results

3.1. Estimation of PWDI

According to measured soil matric potential distributions and a generalized NRLD function (Eq. (5)), daily PWDI under each deficit irrigation treatment (T2-T6 in 2015 and T8-T13 in 2016) during the post-greening period of winter wheat was estimated with Eq. (3), and compared to the measured value in Fig. 2. As defined, the measured PWDI was computed as the ratio of water deficit (T_p - T_a) and water demand T_p (Woli et al., 2012; Shi et al., 2015), in which T_a under each deficit irrigation treatment was identified as the difference between measured actual evapotranspiration rate from lysimeters and calculated evaporation rate by the modified Penman equation (Ritchie, 1972; Wu et al., 2017). T_p was determined by calibrating the measured transpiration rate under sufficient irrigation (T1 in 2015 and T7 in 2016) to consider the effect of differences in growth levels (reflected using the effective leaf area index) of plants exposed to different water stresses (Wu et al., 2017, 2020). The estimated PWDI under each deficit irrigation treatment decreased immediately following irrigation, and then increased gradually due to the loss of soil water by evapotranspiration until the next irrigation (Fig. 2), in good agreement with the measured value with an overall determination coefficient (R^2), Nash-Sutcliffe efficiency coefficient (NSE) and root mean squared error (RMSE) of 0.78, 0.77 and 0.10, respectively (Table 4).

3.2. Parameterization of CWPF

During the period from sowing to greening, sufficient water was supplied for winter wheat in the field lysimetric experiment. The CWPF was constructed for the duration between greening and maturity. The estimation of PWDI in 2015 and 2016 started from 198 and 188 DAS, respectively, due to the lack of some SWC measurements at the early greening period (166–197 DAS in 2015 and 166–187 DAS in 2016). The missing estimated daily PWDIs, which were needed for constructing CWPF, were supplied by their corresponding measured values (Fig. 2).

In CWPF (Eq. (2)), the potential yield (Y_p) was approximated to be the average ($10.7 \times 10^3\ kg\ ha^{-1}$) of the measured yields under sufficient irrigation treatments T1 and T7. Daily sensitivity index (λ_t) was estimated according to Eqs. (6) - (8), where three fitting parameters k, b and m in Eq. (6) were optimized by a nonlinear least-squares method as: k = 23.38, b = 3.53 and m = 1.04 (Table 3). The changing processes of cumulative (C_t) and daily (λ_t) sensitivity index with normalized heat unit index (H_t) are shown in Fig. 3. As designed, an S-shaped C_t naturally generated a low-high-low bell shape of λ_t. The value of λ_t reached its peak of 0.023 at H_t = 0.71, with corresponding C_t = 0.56. With the optimized parameters, Y_a under different irrigation treatments were estimated using the CWPF and compared well with the measured values (Fig. 4), with a R^2 of 0.84, NSE of 0.79, RMSE of 776 $kg\ ha^{-1}$, and a normalized RMSE of 0.098, respectively.

3.3. Optimization of irrigation scheduling for winter wheat

3.3.1. Simulation of soil water flow in the soil-wheat system

The information on soil water dynamics, simulated through Eqs. (9) - (12), is necessary for calculating PWDI. To test the reliability of the

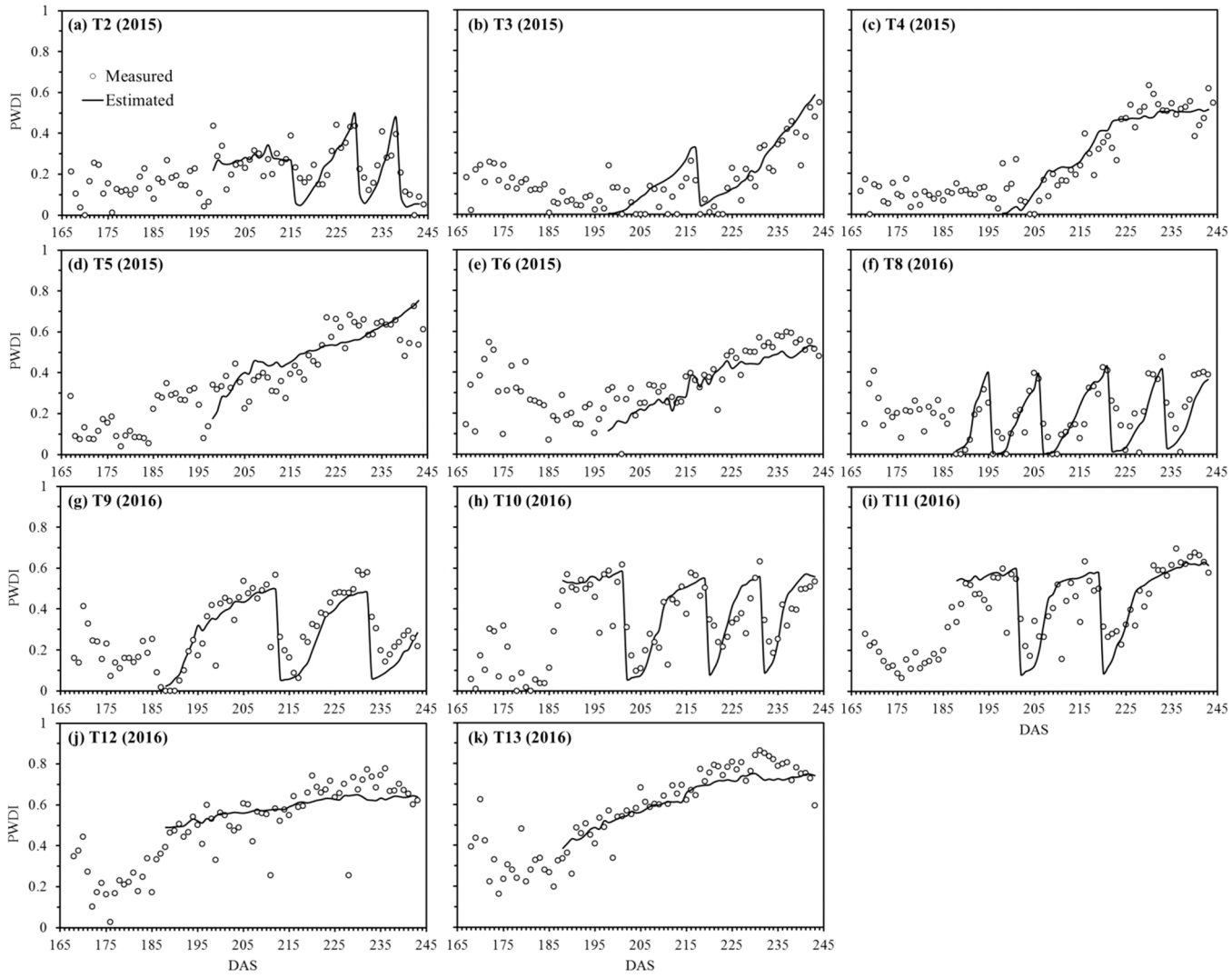

Fig. 2. Comparisons of the measured and estimated daily plant water deficit index (PWDI) based on root-weighted soil water availability under various deficit irrigation treatments (T2-T6 and T8-T13) in two growing seasons (2015 and 2016). DAS = days after sowing.

Table 4
The determination coefficient (R^2), Nash-Sutcliffe efficiency coefficient (NSE) and root mean squared error (RMSE) between the measured and estimated plant water deficit index (PWDI) based on root-weighted soil water availability under various deficit irrigation treatments (T2-T6 and T8-T13) in two growing seasons of 2015 and 2016.

Treatments	R^2	NSE	RMSE
T2 (2015)	0.53	0.11	0.10
T3 (2015)	0.68	0.55	0.10
T4 (2015)	0.76	0.74	0.09
T5 (2015)	0.54	0.41	0.11
T6 (2015)	0.71	0.61	0.08
T8 (2016)	0.67	0.60	0.09
T9 (2016)	0.71	0.63	0.10
T10 (2016)	0.61	0.29	0.12
T11 (2016)	0.57	0.30	0.12
T12 (2016)	0.42	0.32	0.10
T13 (2016)	0.83	0.81	0.06
Overall	0.80	0.77	0.10

model, treatments T3 and T5 from the first growing season, and T9 and T11 from the second growing season were chosen to simulate the dynamics of SWC distributions during the period from greening to maturity of winter wheat. Eqs. (9) - (12) were solved numerically using the

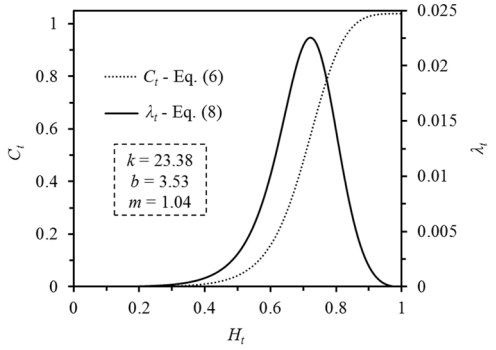

Fig. 3. Cumulative (C_t) and daily (λ_t) water stress sensitivity index as a function of normalized heat unit index (H_t). k, b and m are fitting parameters.

implicit finite difference scheme (Wu et. al, 2021). In the simulation, the SWC profile measured at greening (168 DAS) was used as the initial condition; the upper boundary condition was specified as the evaporation or infiltration rate; the lower boundary condition (L = 100 cm) was determined by the linear interpolation of two successive soil water measurements during the simulation process. The results showed that, whether in soil layer of 0–30 cm or 30–60 cm, under various irrigation

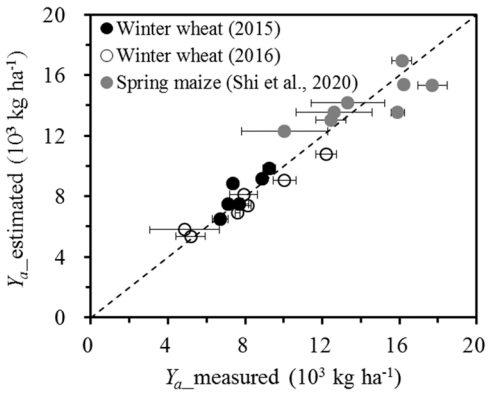

Fig. 4. Measured and estimated actual yields (Y_a) of winter wheat in the field lysimetric experiment and spring maize in the field drip irrigation experiment from Shi et al. (2020) based on respectively parameterized crop-water production functions. Horizontal error bars indicate standard error.

treatments, the simulated average SWCs were found to match the measurements well (Fig. 5a – d), with the RMSE consistently less than 0.03 cm^3 cm^{-3}, and R^2 and NSE greater than 0.86 and 0.53, respectively. The established model therefore appeared to be reliable and reasonable for simulating soil water flow in the soil-wheat system.

3.3.2. *Effects of the irrigation schemes controlled by constant and variable PWDI threshold*

When constant PWDI thresholds were maintained over the period from greening to maturity, gradual increase in their values from 0.01 to 0.99 with an interval of 0.01 led to decrease in the number of simulated irrigation events (and total irrigation depth) from 86 times (52.7 cm) to zero (Fig. 6a). Under the fixed irrigation events (corresponding to different PWDI thresholds, as shown by the dashed rectangle in Fig. 6a), total irrigation depth was found to increase with increasing PWDI threshold. Simulated relationships between PWDI threshold and relative yield (Y_r), and relative irrigation water use efficiency (IWUE$_r$) are shown in Fig. 6b. Increasing PWDI threshold (corresponding to gradually more serious crop water stress) caused Y_r to decline from a maximum close to 1 to a minimum of 0.39 when PWDI threshold = 0.99. Changes in IWUE$_r$ were more complicated. The changing process of IWUE$_r$ vs. PWDI threshold could generally be divided into two stages. At the first stage when the threshold was less than 0.90, IWUE$_r$ increased gradually from a minimum of 0.39 (corresponding IWUE = 2.26 kg m^{-3}) at threshold of 0.01 to a maximum of 1.00 (5.79 kg m^{-3}) at threshold of 0.90. At the second stage IWUE$_r$ rapidly decreased to 0.69 (3.99 kg m^{-3}) at threshold of 0.94 (no calculation required for IWUE$_r$ at the threshold of $>$ 0.94 due to the lack of irrigation event (Fig. 6a)). Additionally, IWUE$_r$ was observed to change periodically with irrigation events, showing a gradual deceasing trend with increasing PWDI threshold in each cycle with fixed irrigation events.

Through the procedure based on GA, the variable PWDI threshold combinations for triggering irrigation events were optimized, and thereupon a corresponding irrigation quantity for each event (Eq. (16)), final Y_r (Eq. (2)) and IWUE$_r$ (Eq. (17)) was obtained (Table 5). In general, both total irrigation depth (the sum of each irrigation quantity) and Y_r increased, but IWUE$_r$ decreased with increasing number of irrigation events due to gradually improved water supply and thus reduced water deficit. Specifically, for a single irrigation event, the PWDI threshold {irrigation quantity} was optimized as 0.90 {11.19 cm} at H_t = 0.70 (corresponding to around flowering-filling stage), leading to a Y_r of 0.53 and an IWUE$_r$ of 1.00. For two irrigation events, the PWDI threshold {irrigation quantity} combination was optimized as [0.86, 0.36] and {[10.08, 9.20 cm]}, corresponding to around late jointing stage (H_t = 0.55) and flowering-filling stage (0.68), and a Y_r of 0.77 and an IWUE$_r$ of 0.84 were obtained. Note that square brackets [] are used to denote PWDI threshold and irrigation quota combinations or vectors, and curly brackets {} distinguish irrigation quota from PWDI threshold. For three irrigation events, the PWDI threshold combination was optimized as [0.80, 0.46, 0.35] {[9.25, 8.69, 8.60 cm]}, corresponding to around middle jointing stage (H_t = 0.47), booting-heading stage (0.57) and flowering-filling stage (0.70), and Y_r increased to a higher level of 0.84 but IWUE$_r$ decreased to a smaller value of 0.67. For four irrigation events, the PWDI threshold combination was optimized as [0.55, 0.48, 0.19, 0.25] {[8.02, 8.05, 7.37, 7.62 cm]}, corresponding to around early jointing stage (H_t = 0.41), late jointing stage (0.51), booting-heading stage (0.59) and flowering-filling stage (0.71), which generated the highest Y_r of 0.88 but lowest IWUE$_r$ of 0.60 among four designed irrigation scenarios.

In comparison with the results from variable PWDI thresholds, corresponding Y_r, IWUE$_r$, and other related optimization parameters such as the value of PWDI threshold, H_t, and irrigation quantity based on a

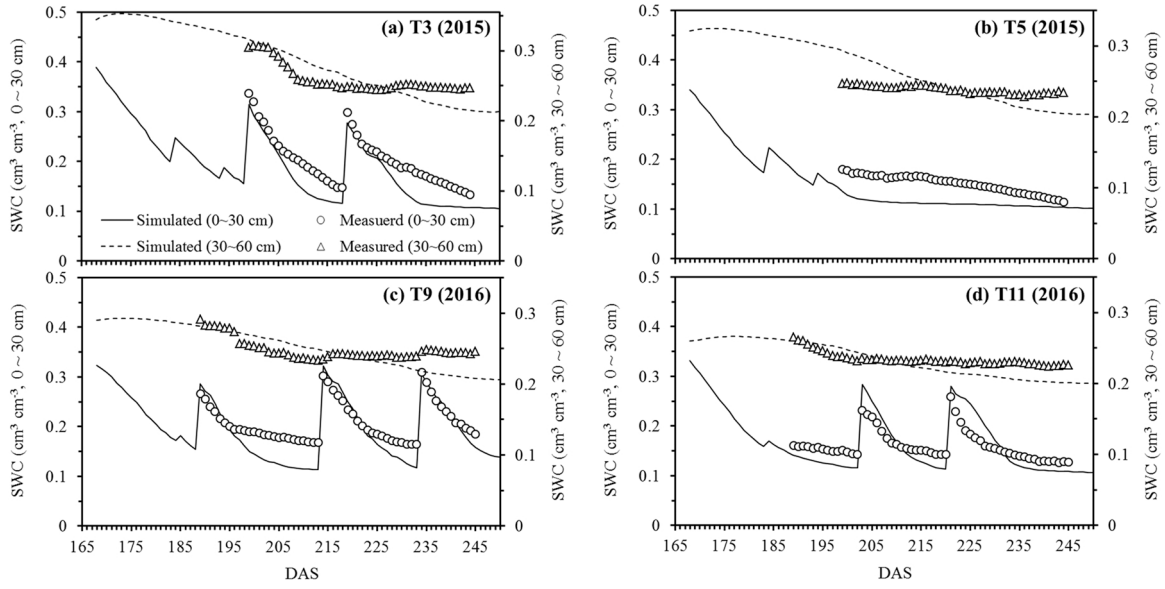

Fig. 5. Measured and simulated average soil water contents (SWCs) at depths of 0–30 cm and 30–60 cm under treatments (a) T3 and (b) T5 in 2015, and (c) T9 and (d) T11 in 2016. DAS = days after sowing.

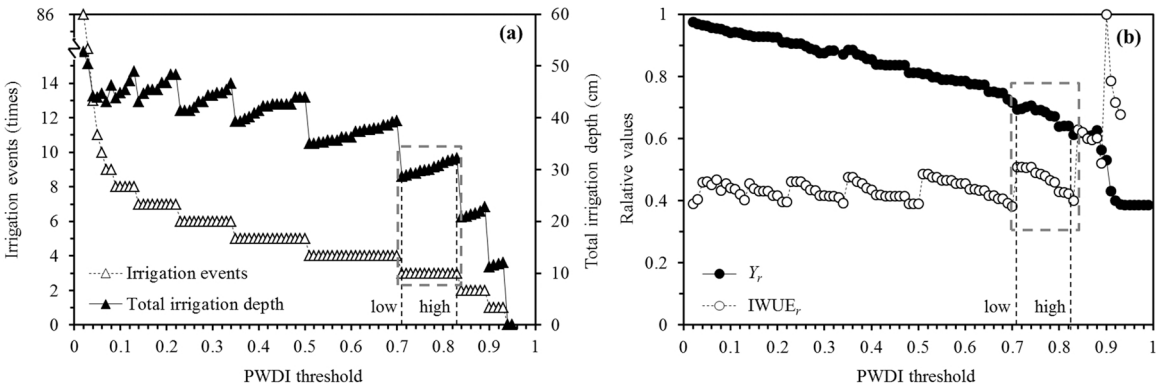

Fig. 6. Simulated (a) irrigation events and total irrigation depth; and (b) relative grain yield (Y_r) and irrigation water use efficiency (IWUE$_r$) as a function of constant PWDI threshold value. The labels "low" and "high" represent the relatively low and high PWDI thresholds for fixed number of irrigation events (e.g. 3 events), respectively.

Table 5
The plant water deficit index (PWDI) threshold combinations, timing of irrigation represented by the normalized heat unit index (H_t), irrigation quota combinations, final relative yields (Y_r), and irrigation water use efficiencies (IWUE$_r$) triggered with constant (low or high for a fixed number of irrigation events) or variable PWDI threshold, respectively. (EJ: early jointing stage; MJ: middle jointing stage; LJ: late jointing stage; BH: booting-heading stage; FF: flowering-filling stage; FI: filling stage; MA: mature stage).

Number of irrigation events	Threshold types	Threshold combination	H_t → growth stage	Irrigation quota (cm)	Y_r	IWUE$_r$
One	–	[0.90]	[0.70] → [FF]	[11.19]	0.53	1.00
Two	Variable	[0.86, 0.36]	[0.55, 0.68] → [LJ, FF]	[10.08, 9.20]	0.77	0.84
Two	Constant (low)	[0.84, 0.84]	[0.51, 0.75] → [LJ, FI]	[9.78, 11.03]	0.62	0.63
Two	Constant (high)	[0.89, 0.89]	[0.68, 0.95] → [FF, MA]	[10.98, 11.85]	0.61	0.60
Three	Variable	[0.80, 0.46, 0.35]	[0.47, 0.57, 0.70] → [MJ, BH, FF]	[9.25, 8.69, 8.60]	0.84	0.67
Three	Constant (low)	[0.71, 0.71, 0.71]	[0.43, 0.57, 0.79] → [EJ, BH, FI]	[8.49, 9.53, 10.69]	0.69	0.51
Three	Constant (high)	[0.83, 0.83, 0.83]	[0.49, 0.74, 0.99] → [MJ, FI, MA]	[9.54, 10.94, 11.68]	0.61	0.40
Four	Variable	[0.55, 0.48, 0.19, 0.25]	[0.41, 0.51, 0.59, 0.71] → [EJ, LJ, BH, FF]	[8.02, 8.05, 7.37, 7.62]	0.88	0.60
Four	Constant (low)	[0.51, 0.51, 0.51, 0.51]	[0.40, 0.52, 0.66, 0.81] → [EJ, LJ, FF, FI]	[8.02, 8.34, 8.89, 9.73]	0.81	0.49
Four	Constant (high)	[0.70, 0.70, 0.70, 0.70]	[0.43, 0.56, 0.77, 0.99] → [EJ, BH, FI, MA]	[8.49, 9.38, 10.40, 11.14]	0.72	0.38

constant PWDI threshold including both low and high values for a fixed number of irrigation events are also shown in Table 5. When the number of irrigation events was fixed as 2, 3, and 4, Y_r (IWUE$_r$) was 24–26% (33–40%), 22–38% (31–68%) and 9–22% (22–58%) higher than those with low-high constant threshold, respectively.

3.3.3. *Optimization of variable PWDI threshold combinations under different climatic conditions*

The effects of varying meteorological conditions due to climate change on the optimization results of variable PWDI threshold combinations were investigated and evaluated by numerical simulation using the optimization procedure according to the historic meteorological data in the study area from 1981 to 2018. The numerical simulation for each growth season included four irrigation schemes with 1–4 irrigation events starting from the field measured SWC distribution at greening stage in 2016. By running the optimization procedure repeatedly as presented in Fig. 1, maximum relative crop yield ($Y_{r,\ max}$) and corresponding optimal PWDI threshold (PWDI$_{opt}$) combinations for four different irrigation schemes were simulated for all the 38 growing seasons. The $Y_{r,\ max}$ and precipitation (P_r) during the growing season (between greening and maturity) of winter wheat over the 38 years from 1981 to 2018 are shown in Fig. 7. The changing tendency of $Y_{r,\ max}$ was found to be positively correlated to P_r with the Pearson correlation coefficient varying between 0.69 and 0.77 ($P < 0.01$), independent of number of irrigation events. In addition, $Y_{r,\ max}$ increased with increasing number of irrigation events, but its increasing rate tended to slow down gradually. For example, the average $Y_{r,\ max}$ (0.70) for a single irrigation over the 38 years was 15.7%, 20.5% and 23.9% respectively lower than those for two (0.83), three (0.88) or four (0.92) irrigation events.

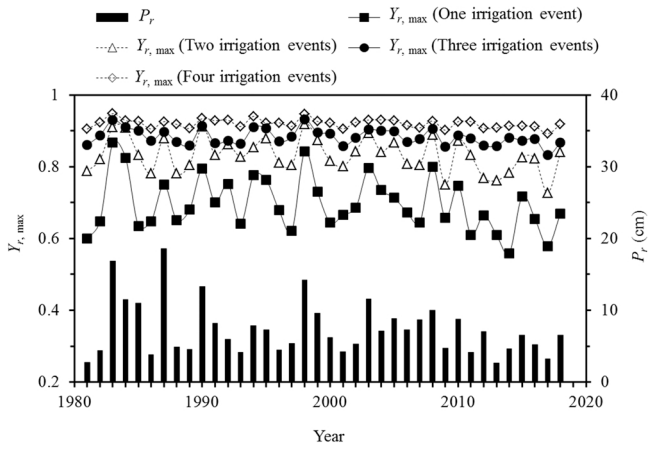

Fig. 7. The optimized maximum relative crop yield ($Y_{r,\ max}$) for different number of irrigation events (i.e. one, two, three or four), and the precipitation (P_r) during the growth season (between greening and maturity) of winter wheat over the 38 years from 1981 to 2018.

Frequency analysis results of precipitation data showed that the 38 years were comprised of nine wet years (e.g. 1987, 1998, 2008) with precipitation frequency $P = 0$–25%, 20 normal years (e.g. 1991, 2002, 2018) with $P = 25$–75% and nine dry years (e.g. 1982, 1986, 2013) with $P = 75$–100%. The relationship between optimized PWDI threshold (PWDI$_{opt}$) and frequency P was influenced by both irrigation sequence and number of irrigation events (Fig. 8a–j). For each combination of irrigation sequence and number of irrigation events, all the values of

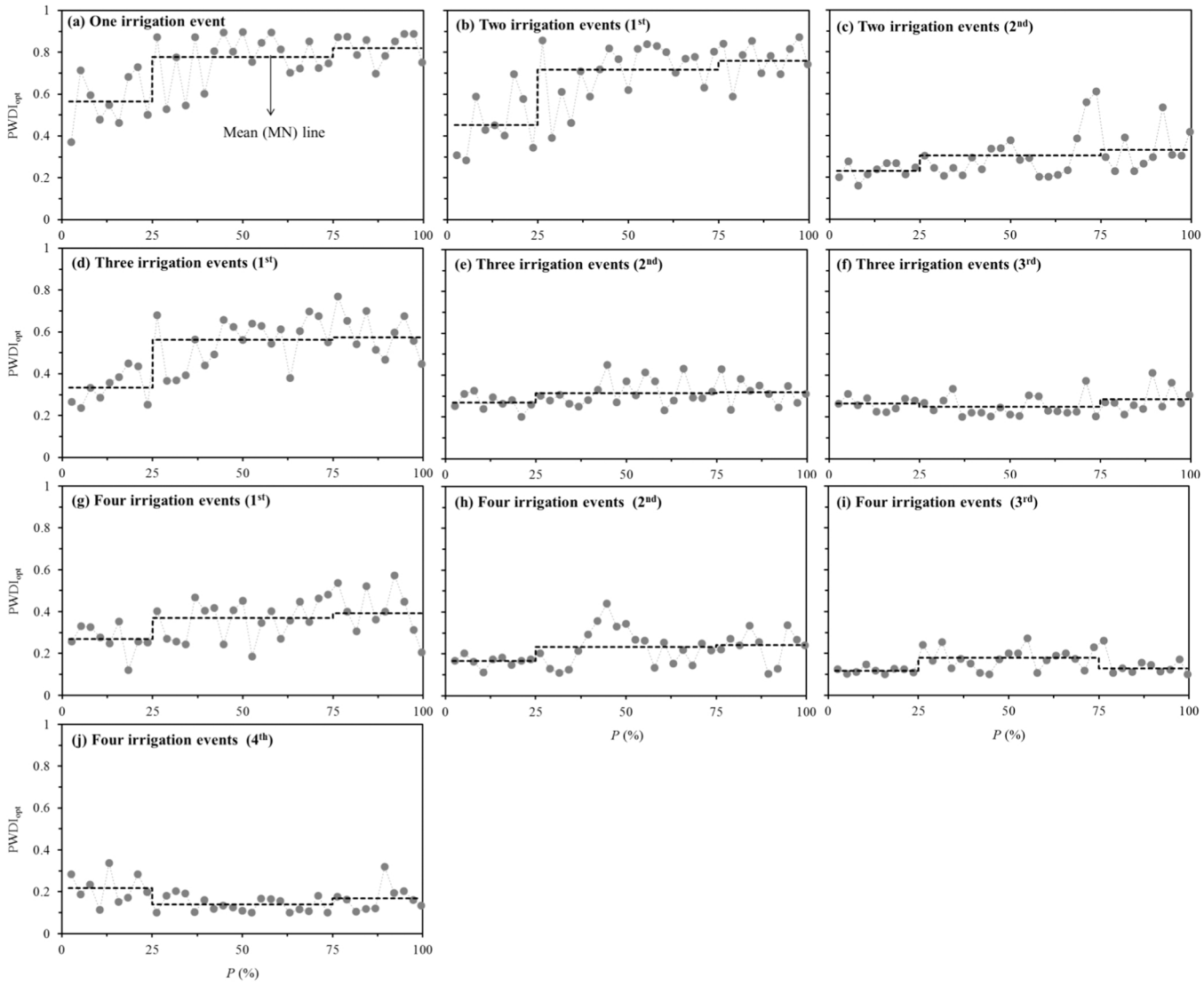

Fig. 8. Optimized plant water deficit index threshold ($PWDI_{opt}$) and precipitation frequency (P) for each sequence of irrigation (e.g. 1st, 2nd, 3rd or 4th irrigation) for different numbers of irrigation events (a) one, (b-c) two, (d-f) three and (g-j) four.

$PWDI_{opt}$ in the same type of hydrological year were averaged and shown in Fig. 8a–j with a dashed line. Irrespective of how many irrigation events winter wheat received after the greening stage, the mean $PWDI_{opt}$ of the 1st irrigation increased to a higher level when P rose from 0% to 25% to 25–75% (viz. with decreasing precipitation and increasing drought degree), and then tended to be approximately stable at the second rising round of P from 25% to 75% to 75–100% (Figs. 8a, 8b, 8d, 8g). A similar trend was observed for the mean $PWDI_{opt}$ of the 2nd

Table 6
The mean (MN) and coefficient of variation (CV) of optimal plant water deficit index thresholds (PWDIopt) for each combination of irrigation sequence and number of irrigation events under three typical types of hydrological year as wet (with precipitation frequency P = 0–25%), normal (25–75%) and dry (75–100%) over the 38 years (in which n denotes the total number of a specific type of hydrological year).

Number of irrigation events	P (%)	1st irrigation		2nd irrigation		3rd irrigation		4th irrigation	
		MN	CV	MN	CV	MN	CV	MN	CV
One	0–25 (n = 9, wet)	0.56	0.22						
	25–75 (n = 20, normal)	0.78	0.15						
	75–100 (n = 9, dry)	0.82	0.08						
Two	0–25 (n = 9, wet)	0.45	0.31	0.23	0.16				
	25–75 (n = 20, normal)	0.72	0.18	0.30	0.31				
	75–100 (n = 9, dry)	0.76	0.12	0.33	0.30				
Three	0–25 (n = 9, wet)	0.33	0.24	0.27	0.14	0.26	0.12		
	25–75 (n = 20, normal)	0.56	0.21	0.31	0.21	0.25	0.19		
	75–100 (n = 9, dry)	0.57	0.16	0.32	0.16	0.29	0.22		
Four	0–25 (n = 9, wet)	0.27	0.25	0.17	0.15	0.12	0.12	0.22	0.33
	25–75 (n = 20, normal)	0.37	0.26	0.23	0.38	0.18	0.29	0.14	0.26
	75–100 (n = 9, dry)	0.39	0.29	0.24	0.33	0.13	0.19	0.17	0.39

irrigation but the increment of its first rising round was greatly reduced (Figs. 8c, 8e, 8h), while little change was observed for the mean $PWDI_{opt}$ of the 3rd or 4th irrigation with P value (Figs. 8f, 8i, 8j). In addition, when irrigated with 2, 3 or 4 events, the mean $PWDI_{opt}$ of the 1st irrigation (Figs. 8b, 8d and 8g) was much higher than those of other sequential irrigations (Figs. 8c, 8e–f and 8h–j).

Both mean (MN) and coefficient of variation (CV) of $PWDI_{opt}$ for each combination of irrigation sequence and number of irrigation events under different types of hydrological year are listed in Table 6. For each sequential irrigation event, the highest MN was almost always in dry years with the least precipitation but lowest in wet years. All the calculated CV varied between 0.08 and 0.39, with a median of 0.21.

4. Discussion

4.1. PWDI estimation and CWPF evaluation

Root-weighted PWDI estimation seems to provide a reliable method to evaluate the extent of crop water deficit (Fig. 2, Table 4). One explanation for its success probably lies in its rigorous consideration of the effect of relative distribution patterns of soil water to roots on crop water use (Shi et al., 2015; Wu et al., 2017). Nevertheless, the estimated PWDI failed to match a few fluctuations of measured PWDI, likely resulting from occasionally sharp changes of a meteorological variable such as solar radiation (Wu et al., 2017) or the unavoidable hysteresis effect of previous water stress on transpiration (Wu et al., 2020, 2021). For example, the measured PWDIs under treatment T12 on 211 and 228 DAS (0.25 and 0.26) were observed to be obviously lower than their estimated values (0.60 and 0.67, Fig. 2j). This is presumably explained by the sudden decrease of solar radiation from 11.7 and 15.1 MJ m^{-2} d^{-1} on the previous days to 2.9 and 2.2 MJ m^{-2} d^{-1}, respectively, leading to the lowest R^2 of 0.42 among all the irrigation treatments (Table 4). In addition, different from the estimated PWDIs simultaneously and sharply decreasing close to zero after re-watering on 216, 230 and 239 DAS due to abruptly improved soil water status, the measured PWDIs at the post-irrigation corresponding durations of 216–218, 230–233, and 239–242 DAS under treatment T2 tended to decline gradually and deviate far from the estimated values (Fig. 2a), thus leading to the lowest NSE of 0.11. We attribute this phenomenon when plant response lags behind water status changes in soil, and is therefore hard to predict, mainly to the hysteresis effect of previous water stress (Anderegg et al., 2015; Wu et al., 2021). In order to represent crop water deficit degree more accurately, the effects of weather changes as well as plant hysteresis dynamics after re-watering resulting from drought stress should therefore be taken into account.

Parameterization (Eq. (6)) revealed that the largest increased rate of C_t, equivalent to the highest λ_t, was situated at $H_t = 0.71$ (Fig. 3), corresponding to the flowering-filling stage of winter wheat. Such indication that the flowering-filling stage is the most sensitive period of winter wheat to water stress is consistent with many other reported results (Li, 1990; Zhang and Oweis, 1999). The root-weighted soil water availability based PWDI (used to represent real-time crop water deficit extent) combined with the daily sensitivity index generated from cumulative function (used to describe crop water sensitivity dynamics during crop growing season) established a novel CWPF providing a reasonable and reliable prediction for winter wheat yield under various levels of water supply (Fig. 4).

In order to further verify the reliability of the proposed CWPF construction method under different conditions, we utilized data from a two-year field drip irrigation experiment conducted in Inner Mongolia, China published in Shi et al. (2020), to parameterize the CWPF for spring maize grown in a sandy soil. Eight treatments with various water supply levels were evaluated in the experiment. Different from the linear form demonstrated in Eq. (4), a nonlinear soil water stress response function was necessary to estimate the PWDI for each treatment in the Shi et al. (2020) experiment. Based on the parameterized CWPF with $k = 1.47$, $b = 5.90$ and $m = 0.68$ for Eq. (6), the spring maize yields were estimated under various water supply treatments and compared with the measured values (Fig. 4). The results showed good agreement between measured and estimated actual maize yield (Fig. 4) with a R^2 of 0.61, NSE of 0.57, and normalized RMSE of 0.11. The success of the method for both winter wheat and spring maize, representing crops with different water stress response characteristics (linear and non-linear) under different environments (soil type, climate zone and irrigation method) raises our confidence in the reliability and applicability of the proposed method of CWPF construction to accurately evaluate crop yields generally.

4.2. Irrigation scheduling using optimized constant and variable PWDI thresholds

One potentially important use of the established CWPF is to determine optimal irrigation timing using PWDI thresholds to trigger irrigation events (Osroosh et al., 2015; Shi et al., 2020). When the PWDI threshold was kept constant throughout the growing season, the incremental PWDI threshold generally resulted in a smaller number of simulated irrigation events (and less total irrigation depth), as a function of prolonged duration between two successive irrigation events (Fig. 6a). For a fixed irrigation event, the positive relationship between total irrigation depth and PWDI threshold (Fig. 6a) can be explained by higher PWDI thresholds resulting in greater soil water deficit in the root zone prior to irrigation, and that more irrigation water was required to achieve the target water content (viz. field water capacity, Eq. (16)).

Besides irrigation scheduling, crop yield and WUE are also influenced by many other factors such as weather, crop variety, and field management. Normalizing the yield and WUE by their respective maximum values may be helpful to avoid the impact from other factors to a certain extent and reasonably evaluate the effects of irrigation (Zheng et al., 2012; Shi et al., 2021). The increasing trend of relative irrigation water use efficiency ($IWUE_r$) at the first stage when the threshold ≤ 0.90 (Fig. 6b) was likely due to the faster declining rate of total irrigation depth (Fig. 6a) relative to yield (Fig. 6b). At the later stage when threshold > 0.90, the rapidly declining $IWUE_r$ resulted conversely from the sharply dropping crop yield due to severe water deficit (Fig. 6b). In each cycle with fixed irrigation events, $IWUE_r$ decreased slowly with increasing PWDI threshold values (Fig. 6b), as a result of the incremental increase in total irrigation depth (Fig. 6a) but declining crop yield (Fig. 6b) according to Eq. (17).

The main shortcoming of scheduling irrigation with a constant PWDI threshold is that the sensitivity of crop yield to water deficit is assumed to be constant throughout the growing season. Thus, the effect of the difference in water sensitivity of different growth stages on the optimization of PWDI threshold is ignored (Shi et al., 2020, 2021). The procedure based on GA overcame this shortcoming by globally optimizing the variable PWDI threshold combinations for triggering irrigation events. The optimization results showed that the prime timing for variable irrigation events occurred during the period between jointing and filling stages of winter wheat, especially in flowering-filling stage (Table 5), which should be critical to yield formation of the crop (Li, 1990; Zhang et al., 1999). In other words, sufficient water supply during this stage is essential for maximizing crop yield irrespective of the number of irrigation events during the complete growing season. Relative to the constant threshold, there was obvious superiority of regulated deficit irrigation (RDI) triggered with a variable threshold in improving both Y_r and $IWUE_r$ (Table 5). This suggests that full consideration of water demand characteristics of crops at different growth stages, and thus reasonable allocation of irrigation water is desired and possible (Foster and Brozovi, 2018; Shi et al., 2021). However, these conclusions may be biased due to being based on numerical simulation results obtained only from a controllable field lysimetric experiment for winter wheat during a specific growing season when natural rainfall was prevented by a movable rain-shelter.

4.3. Effects of climate change

The effects of climate change on optimized variable PWDI threshold combinations and maximum relative yield of winter wheat ($Y_{r,\ max}$) were investigated based on historic meteorological data. The positive correlation between the optimized $Y_{r,\ max}$ of winter wheat and P_r in the 38 growth seasons (Fig. 7) indicated that natural precipitation has a significant impact on the potential yield of winter wheat. The gradually waning increasing rate of $Y_{r,\ max}$ from one to four irrigation events (Fig. 7) demonstrated a significant diminishing return for irrigation (Foster and Brozovi, 2018; Li et al., 2018a, 2018b).

Whether for 2, 3 or 4 irrigation events, the highest mean $PWDI_{opt}$ (optimal plant water deficit index threshold) was always found under the 1st irrigation (Fig. 8b–j), mainly because the 1st irrigation was basically conducted during the period from erecting to jointing stage (with H_t of about 0.35–0.45) of winter wheat when its sensitivity to water was relatively low (Fig. 3). Therefore, continuous water consumption by evapotranspiration would inevitably lead to significant reduction of root-zone SWC and in further increase of PWDI. During the later period, from jointing to filling stages (with H_t = 0.45–0.75), the significantly enhanced crop water sensitivity (Fig. 3) resulted in relatively more sufficient water supply and thus lower mean $PWDI_{opt}$ between 0.12 and 0.33 for the 2nd, 3rd and 4th irrigation (Figs. 8c, 8e-8f, 8h-8j).

The values of MN and CV (Table 6) represent the statistical characteristics of $PWDI_{opt}$ under three typical types of hydrological year. For a fixed combination of irrigation sequence (1st, 2nd, 3rd, or 4th) and number of irrigation events (1−4), most MNs were observed to decrease with decreasing P (i.e. from dry to normal and then to wet years), except for the very few cases with higher irrigation sequence and number of irrigation events (e.g. the 3rd and 4th irrigation under four irrigation events), which were likely affected by local uncertainty of meteorological factors (e.g. precipitation, air temperature, solar radiation, etc.) among and within different types of hydrological years. The variability of $PWDI_{opt}$ for different combinations of irrigation sequence and events under the same kind of hydrological year likely originated from the uncertainty or stochasticity of hydrological elements such as precipitation and evapotranspiration, the important driving factors of soil water dynamics and PWDI estimation. Because of the inherent huge uncertainty of the climate, the variability represented by CV < 0.39 is generally considered to be small (Kassie et al., 2014). Therefore, it should be reasonable to ignore the differences of $PWDI_{opt}$ among various growth seasons under the same type of hydrological year, and apply the calculated MN to support local irrigation decisions and meet agricultural water management requirements.

To examine the applicability of the MN listed in Table 6, all 30 values of MN for different irrigation sequence and number of irrigation events were used to replace the originally optimized variable PWDI threshold combinations (Fig. 8) of the 38 growth seasons from 1981 to 2018 according to their classification of hydrological year. Thereafter, they were applied to trigger irrigation during the simulation of soil water flow and estimate the relative yield ($Y_{r,\ est}$) of winter wheat using the integrated optimization procedure via the coupling of the Richards equation, CWPF and GA. The values of $Y_{r,\ est}$ from one, two, three or four irrigation events in the 38 years were compared with corresponding maximum relative crop yields $Y_{r,\ max}$ (Fig. 7, optimized using the original variable PWDI threshold combinations) in Fig. 9, in which the percentages (80%, 90%, 95% or 100%) represent the ratio of $Y_{r,\ est}$ to $Y_{r,\ max}$. The results show that all $Y_{r,\ est}$ estimated based on the MN were above the level of 80% $Y_{r,\ max}$, and the percentage of $Y_{r,\ est}$ exceeding 90% (95%) of $Y_{r,\ max}$ reached up to 91% (85%). The degree of closeness of $Y_{r,\ est}$ to $Y_{r,\ max}$ increased significantly with increasing number of irrigation events. For example, the proportion of $Y_{r,\ est}$ exceeding 95% of $Y_{r,\ max}$ was 69%, 81%, 96% and 98% for one, two, three, and four events, respectively. Obviously, MN-based $Y_{r,\ est}$ was comparable with $Y_{r,\ max}$ in most cases, especially when three or four irrigation events were applied, which exactly reflects

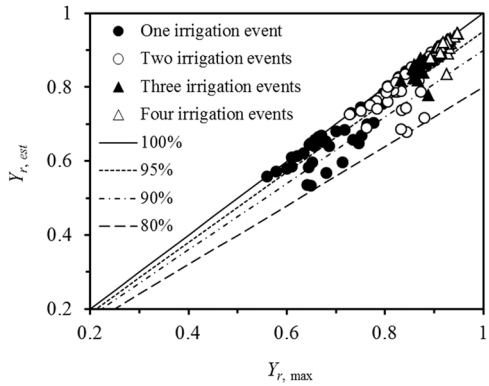

Fig. 9. Comparisons of the relative yield ($Y_{r,\ est}$) estimated based on combinations of the mean of originally optimized plant water deficit index (PWDI) thresholds and the maximum relative yield ($Y_{r,\ max}$) directly estimated with combinations of the originally optimized PWDI thresholds. The percentage (80, 90, 95, 100%) represents the ratio of $Y_{r,\ est}$ and $Y_{r,\ max}$.

common practice in agricultural water management in the North China Plain (Yang et al., 2014). Therefore, the values of MN in Table 6 can be recommended as variable PWDI threshold combinations to schedule RDI as a function of number of irrigation events and type of hydrological year, which should be helpful for maximizing water use efficiency, particularly when water supply is limited and deficit irrigation strategies are necessary. However, it should be noted that the optimized MN might be very different from its theoretical or true threshold as a result of the possibly dramatic variation of intra and inter annual meteorological conditions in practice, especially under actual field conditions. Further practical research is needed to introduce uncertainty estimation methods such as stochastic, fuzzy and interval mathematical programming into the optimization procedure to more rationally reflect the impact of climate change and the complexity of irrigation systems (Li et al., 2018a, 2018b).

5. Conclusions

A novel crop-water production function (CWPF) was proposed by combining root-weighed soil water availability based PWDI with daily water sensitivity index derived from a sigmoidal cumulative function. Whether parameterized using data from a winter wheat field lysimetric experiment conducted in the North China Plain or a spring maize field drip irrigation experiment in Inner Mongolia, China, the CWPF reasonably estimated crop yields under various deficit irrigation treatments, with the R^2 not less than 0.61, NSE not less than 0.57 and normalized RMSE not more than 0.11 between the measured and estimated values. By coupling the genetic algorithm with the verified integrated simulations of soil water dynamics, PWDI and CWPF, an optimization procedure was developed to determine a PWDI threshold combination for winter wheat, whether constant or variable, and to investigate the effects of climate change on optimized variable PWDI threshold combinations based on 38 years of local historic meteorological data. Relative to the constant threshold, RDI initiated with a variable threshold resulted in a significant increase of 9–38% in crop yield and 31–68% in IWUE due to the consideration of relative sensitivity of crop yield to water deficit at different growth stages. Regardless of how many times winter wheat was irrigated after the greening stage, the variability of optimized PWDI thresholds among various growth seasons under the same kind of hydrological year (wet, normal or dry) was not very large (CV < 0.39) and might be negligible in many practical cases. When the mean values of optimized PWDI thresholds for different irrigation sequence and number of irrigation events were used to schedule RDI of winter wheat under the same kind of hydrological year, up to 91% of the estimated relative yields exceeded 90% of their

corresponding maximums, with the closeness degree between them increased with increasing number of irrigation events. The mean values appear to be a valid technique for optimizing irrigation management of winter wheat in the North China Plain. However, further actual field studies regarding rational quantitative description on the uncertainty of meteorological conditions due to climate change and its impacts on PWDI threshold optimization are necessary.

Declaration of Competing Interest

The authors declare that they have no known competing financial interests or personal relationships that could have appeared to influence the work reported in this paper.

Acknowledgements

This research was supported partly by National Natural Science Foundation of China (U1706211, 51790532), National Key Research and Development Program of China (2017YFE0118100), and the European Union's Horizon 2020 research and innovation programme under Project SHui, grant agreement No 773903.

References

Allen, R.G., Pereira, L.S., Raes, D., Smith, M., 1998. Crop evapotranspiration: guidelines for computing crop water requirements. FAO Irrigation and Drainage Paper No. 56. FAO, Rome, Italy.
Anderegg, W.R.L., Schwalm, C., Biondi, F., Camarero, J.J., Koch, G., Litvak, M., Ogle, K., Shaw, J.D., Shevliakova, E., Williams, A.P., Wolf, A., Ziaco, E., Pacala, S., 2015. Pervasive drought legacies in forest ecosystems and their implications for carbon cycle models. Science 349, 528–532.
Arora, V.K., Prihar, S.S., Gajri, P.R., 1987. Synthesis of a simplified water use simulation model for predicting wheat yields. Water Resour. Res. 23, 903–910.
Asseng, S., Richter, C., Wessolek, G., 1997. Modelling root growth of wheat as the linkage between crop and soil. Plant Soil 190, 267–277.
Ben-Gal, A., Karlberg, L., Jansson, P.E., Shani, U., 2003. Temporal robustness of linear relationships between production and transpiration. Plant Soil 251, 211–218.
Candogan, B.N., Sincik, M., Buyukcangaz, H., Demirtas, C., Goksoy, A.T., Yazgan, S., 2013. Yield, quality and crop water stress index relationships for deficit-irrigated soybean [*Glycine max* (L.) Merr.] in sub-humid climatic conditions. Agric. Water Manag. 118, 113–121.
Dabach, S., Lazarovitch, N., Šimůnek, J., Shani, U., 2013. Numerical investigation of irrigation scheduling based on soil water status. Irrig. Sci. 31, 27–36.
Diepen, C.A., Wolf, J., Keulen, H., Rappoldt, C., 1989. WOFOST: a simulation model of crop production. Soil Use Manag. 5, 16–24.
Elliott, J., Deryng, D., Müller, C., Frieler, K., Konzmann, M., Gerten, D., Glotter, M., Flörke, M., Wada, Y., Best, N., et al., 2014. Constraints and potentials of future irrigation water availability on agricultural production under climate change. Proc. Natl. Acad. Sci. USA. 111, 3239–3244. https://doi.org/10.1073/pnas.1222474110.
Emekli, Y., Bastug, R., Buyuktas, D., Emekli, N.Y., 2007. Evaluation of a crop water stress index for irrigation scheduling of bermudagrass. Agric. Water Manag. 90, 205–212.
Feddes, R.A., Kowalik, P.J., Malinka, K.K., Zaradny, H., 1976. Simulation of field water uptake by plants using a soil water dependant root extraction function. J. Hydrol. 31, 13–26.
Feddes, R.A., Kowalik, P.J., Zaradny, H., 1978. Simulation of Field Water Use and Crop Yield. Simulation Monographs Pudoc., Wageningen, The Netherlands.
Foster, T., Brozovi, N., 2018. Simulating crop-water production functions using crop growth models to support water policy assessments. Ecol. Econ. 152, 9–21.
Gee, G.W., Or, D., 2002. Particle size analysis. In: Dane, J., Topp, G.C. (Eds.), Methods of Soil Analysis. Part 4. Physical Methods. ASA and SSSA, Madison, WI, pp. 278–282.
Georgiou, P.E., Papamichail, D.M., 2008. Optimization model of an irrigation reservoir for water allocation and crop planning under various weather conditions. Irrig. Sci. 26, 487–504.
Han, S.J., Liu, Q.H., Wang, S.L., Hu, Y.Q., 2010. Improvement and verification of cumulative function of crop water sensitive index. Trans. CSAE 26, 83–88.
Hanks, R.J., Hill, R.W., 1980. Modelling crop responses to irrigation in relation to soils, climate and salinity. Int. Irrig. Inf. Cent. 66.
Holland, J.H., 1975. Adaption in Natural and Artificial Systems. The University of Michigan Press, Ann Arbor.
Homaee, M., Feddes, R.A., Dirksen, C., 2002. Simulation of root water uptake. II. Nonuniform transient Water Stress Using Differ. Reduct. Funct. Agric. Water Manag. 57, 111–126.
Huang, G.H., 2004. Modeling soil water regime and corn yields considering climatic uncertainty. Plant Soil 259, 221–229.
Igbadun, H.E., Tarimo, A.K.P.R., Salim, B.A., Mahoo, H.F., 2007. Eval. Sel. Crop. Water Prod. Funct. Irrig. maize Crop. Agric. Water Manag 94, 1–10.
Irmak, S., Haman, D.Z., Bastug, R., 2000. Determination of crop water stress index for irrigation timing and yield estimation of corn. Agron. J. 92, 1221–1227.
Jarvis, N.J., 1989. A simple empirical model of root water uptake. J. Hydrol. 107, 57–72.
Jensen, M., 1968. Water consumption by agricultural plants. In: Kozlowski, T. (Ed.), Water Deficits in Plant Growth. Academic Press, New York, USA, pp. 1–22.
Jones, J.W., Hoogenboom, G., Porter, C.H., Boote, K.J., Batchelor, W.D., Hunt, L., Wilkens, P.W., Singh, U., Gijsman, A.J., Ritchie, J.T., 2003. The DSSAT cropping system model. Eur. J. Agron. 18, 235–265.
Kassie, B.T., Van Ittersum, M.K., Hengsdijk, H., Asseng, S., Wolf, J., Rotter, R.P., 2014. Climate-induced yield variability and yield gaps of maize (*Zea mays* L.) in the Central Rift Valley of Ethiopia. Field Crops Res 160, 41–53.
Kipkorir, E.C., Raes, D., 2002. Transform. yield Response Factor into Jensen's Sensit. Index. Irrig. Drain. Syst. 16, 47–52.
Klute, A., Dirksen, C., 1986. Hydraulic conductivity and diffusivity: laboratory methods. In: Klute (Eds.), Methods of Soil Analysis. Part 1. 2nd ed. Agron. Monogra. 9. ASA and SSSA, Madison, WI, USA, pp. 687-734.
Lai, C.T., Katul, G., 2000. The dynamic role of root-water uptake in coupling potential to actual transpiration. Adv. Water Resour. 23, 427–439.
Li, H.C., 1990. Analysis and study on crop sensitivity index and sensitivity coefficient. J. Irri. Dran. 9, 7–14.
Li, J., Song, J., Li, M., Shang, S.H., Mao, X.M., Yang, J., Adeloye, A.J., 2018. Optimization of irrigation scheduling for spring wheat based on simulation-optimization model under uncertainty. Agric. Water Manag. 208, 245–260.
Li, M., Fu, Q., Singh, V., Liu, D., 2018. An interval multi-objective programming model for irrigation water allocation under uncertainty. Agric. Water Manag. 196, 24–36.
Mailhol, J.C., Olufayo, A., Ruelle, P., 1997. Sorghum and sunflower evapotranspiration and yield from simulated leaf area index. Agric. Water Manag. 35, 167–182.
Morgan, T.H., Biere, A.W., Kanemasu, E.T., 1980. A dynamic model of corn yield response to water. Water Resour. Res. 16, 59–64.
Musters, P.A.D., Bouten, W., 1999. A method for identifying optimum strategies of measuring soil water contents for calibrating a root water uptake model. J. Hydrol. 227, 273–286.
Ning, S.R., Shi, J.C., Zuo, Q., Wang, S., Ben-Gal, A., 2015. Generalization of the root length density distribution of cotton under film mulched drip irrigation. Field Crop Res. 177, 125–136.
Ojeda-Bustamante, W., Sifuentes-Ibarra, E., Slack, D.C., Carrillo, M., 2004. Generalization of irrigation scheduling parameters using the growing degree days concept: application to a potato crop. Irrig. Drain. 53, 251–261.
Osroosh, Y., Peters, R.T., Campbell, C.S., Zhang, Q., 2015. Automatic irrigation scheduling of apple trees using theoretical crop water stress index with an innovative dynamic threshold. Comput. Electron. Agric. 188, 193–203.
Oweis, T., Hachum, A., 2009. Optimizing supplemental irrigation: tradeoffs between profitability and sustainability. Agric. Water Manag. 96, 511–516.
Rao, N.H., Sarma, P.B.S., Chander, S., 1988. A simple dated water-production function for use in irrigated agriculture. Agric. Water Manag. 13, 25–32.
Ritchie, J.T., 1972. Model for predicting evaporation from a row crop with incomplete cover. Water Resour. Res. 8, 1204–1213.
Romano, N., Santini, A., 2002. Water retention and storage: Field-field water capacity. In: Dane, J.H., Topp, G.C. (Eds.), Methods of Soil Analysis. Part 4. SSSA Book Ser. No. 5. SSSA, Madison, WI, pp. 723–729.
Shang, S.H., Mao, X.M., 2006. Application of a simulation based optimization model for winter wheat irrigation scheduling in North China. Agric. Water Manag. 85, 314–322.
Shi, J.C., Li, S., Zuo, Q., Ben-Gal, A., 2015. An index for plant water deficit based on root-weighted soil water content. J. Hydrol. 522, 285–294.
Shi, J.C., Wu, X., Wang, X.Y., Zhang, M., Han, L., Zhang, W.J., Liu, W., Zuo, Q., Wu, X.G., Zhang, H.F., Ben-Gal, A., 2020. Determining threshold values for root-soil water weighted plant water deficit index based smart irrigation. Agric. Water Manag. 230, 105979.
Shi, J.C., Wu, X., Zhang, M., Wang, X.Y., Zuo, Q., Wu, X.G., Zhang, H.F., Ben-Gal, A., 2021. Numerically scheduling plant water deficit index-based smart irrigation to optimize crop yield and water use efficiency. Agric. Water Manag. 248, 106774.
Šimůnek, J., Hopmans, J.W., 2009. Modeling compensated root water and nutrient uptake. Ecol. Model. 220, 505–521.
Singh, A., 2014. Simulation-optimization modeling for conjunctive water use management. Agric. Water Manag. 141, 23–29.
Singh, A., Panda, S.N., 2013. Optimization and simulation modelling for managing the problems of water resources. Water Resour. Manag. 27, 3421–3431.
Smilovic, M., Gleeson, T., Adamowski, J., 2016. Crop kites: determining crop-water production functions using crop coefficients and sensitivity indices. Adv. Water Res. 97, 193–204.
Sotomayor, G., Hampel, H., Vázquez, R.F., 2018. Water quality assessment with emphasis in parameter optimisation using pattern recognition methods and genetic algorithm. Water Res. 130, 353–362.
Steduto, P., Hsiao, T.C., Raes, D., Fereres, E., 2009. AquaCrop-The FAO crop model to simulate yield response to water: I. Concepts and underlying principles. Agron. J. 101, 426–437.
Stewart, J.I., Hagan, R.M., 1973. Functions to predict effects of crop water deficits. J. Irrig. Drain. Div. Am. Soc. Civ. Eng. 99, 421–439.
van Genuchten, M.T., 1980. A closed-Form. Equ. Predict. Hydraul. Conduct. Unsatur. Soils Soil Sci. Soc. Am. J. 44, 892–898.
van Genuchten, M.T., 1987. A numerical model for water and solute movement in and below the root zone. Res. Rep. 121. USDAARS, U. S. Salin. Lab., Riverside, CA USA.
Wang, X.X., Wang, Q.J., Fan, J., Fu, Q.P., 2013. Evaluation of the AquaCrop model for simulating the impact of water deficits and different irrigation regimes on the biomass and yield of winter wheat grown on China's Loess Plateau. Agric. Water Manag. 129, 95–104.

Wang, Y.C., Yu, P.S., Yang, T.C., 2010. Comparison of genetic algorithms and shuffled complex evolution approach for calibrating distributed rainfall-runoff model. Hydrol. Process. 24, 1015–1026.
Wen, Y., Shang, S., Yang, J., 2017. Optimization of irrigation scheduling for spring wheat with mulching and limited irrigation water in an arid climate. Agric. Water Manag. 192, 33–44.
Woli, P., Jones, J.W., Ingram, K.T., Fraisse, C.W., 2012. Agric. Ref. Index Drought (ARID). Agron. J. 104, 287–300.
Woli, P., Jones, J.W., Ingram, K.T., Hoogenboom, G., 2014. Predicting crop yields with the agricultural reference index for drought. J. Agron. Crop Sci. 200, 163–171.
Wu, J., Zhang, R., Gui, S., 1999. Modeling soil water movement with water uptake by roots. Plant Soil 215, 7–17.
Wu, X., Zhang, W.J., Liu, W., Zuo, Q., Shi, J.C., Yan, X., Zhang, D., Xue, H.F., Wang, X.Z., Zhang, L.C., Ben-Gal, M., 2017. Root-weighted soil water status for plant water deficit index based irrigation scheduling. Agric. Water Manag. 189, 137–147.
Wu, X., Zuo, Q., Shi, J.C., Wang, L.C., Xue, X.Z., Ben-Gal, A., 2020. Introducing water stress hysteresis to the Feddes empirical macroscopic root water uptake model. Agric. Water Manag. 240, 106293.
Wu, X., Shi, J.C., Zuo, Q., Zhang, M., Xue, X.Z., Wang, L.C., Zhang, T., Ben-Gal, A., 2021. Parameterization of the water stress reduction function based on soil–plant water relations. Irri. Sci. 39, 101–122.
Yang, G., Pu, R., Zhao, C., Xue, X., 2014. Estimating high spatiotemporal resolution evapotranspiration over a winter wheat field using an IKONOS image based complementary relationship and lysimeter observations. Agric. Water Manag. 133, 34–43.
Zhang, H., Oweis, T., 1999. Water-yield relations and optimal irrigation scheduling of wheat in the Mediterranean region. Agric. Water Manag. 38, 195–211.
Zhang, H., Wang, X., You, M., Liu, C., 1999. Water-yield relations and water use efficiency of winter wheat in the North China Plain. Irrig. Sci. 19, 37–45.
Zheng, J., Huang, G., Wang, J., Huang, Q., Pereira, L.S., Xu, X., Liu, H., 2012. Effects of water deficits on growth, yield and water productivity of drip-irrigated onion (*Allium cepa* L.) in an arid region of Northwest China. Irrig. Sci. 31, 995–1008.
Zuo, Q., Zhang, R., Shi, J., 2013. Characterization of the root length density distribution of wheat using a generalized function. In: Timlin, D., Ahuja, L.R. (Eds.), Enhancing Understanding and Quantification of Soil-Root Growth Interactions. American Society of Agronomy Publisher, pp. 93–117.